GSA DATA REPOSITORY 2014375

# Supplement

# Ocean acidification in the aftermath of the Marinoan glaciation

**Frank Ohnemueller, Anthony R. Prave, Anthony E. Fallick, Simone A. Kasemann**

## GEOLOGICAL SETTING

### Yangtze Platform (China)

Precambrian-Cambrian strata are widespread on the Yangtze Platform (Zhang et al., 1997; Zhu et al., 2003). The Three Gorges area is located at the central northern part of the platform, Hubei Province. Platform interior successions are typically comprised of shallow-water carbonates and deep-water shales of Cryogenian to Cambrian age. From oldest to youngest, the Liantuo, Nantuo, Doushantuo, Dengying, Yanjiahe, Shuijingtuo and Shipai Formations (Ma et al., 1984) are exposed in the Three Gorges area. The investigated Xiaofenghe Section (N 30°56.491, E 111°13.957) is located approximately 28 km N of Yichang, crops out along the northern and southern mountainsides of a small valley, and provides access to ~200 m of well exposed strata.

Nantuo Formation glacial diamictites are directly overlain by ~4 m of Doushantuo Formation cap dolomites (Doushantuo I), which can be subdivided by microfacies into C1, C2 and C3 after the classification of Jiang et al. (2003). The lowermost 0.5 m correspond to unit C1 and consist of grey dolostones with minor calcite veining. Up to ~2.5 m a grey, fine laminated, micritic dolostone (C2) with minor cm-scale chert layers is exposed. The uppermost unit (C3) displays a laminated dolostone layer containing teepee-like fluid-escape structures. On top of the cap dolomite are several meters of grey, micritic dolostones interbedded with chert-nodule-

bearing black shales (Doushantuo II Formation). Xiao et al. (2012) suggested the northern Xiaofenghe Section represented a shallow-water, inner shelf environment.

**Karatau microcontinent (Kazakhstan)**

The southern Kazakh Karatau Mountains form the foothills of the Tian Shan orogen and consist of the Bolshoi (NW) and Malyi (SE) Karatau Range that are divided by the Main Karatau Fault (Alexeiev et al., 2009 and references therein). The investigated Kyrshabakty Section (N 43°32'2.1" E 69°57'7.7"), located approximately 18 km E of Zhanatas is part of the Malyi Karatau Range which is surrounded by the Syr Dar'ya Basin to the SW and the Chu Sarysu Basin to the NE (Allen et al., 2001). The complete Precambrian-Cambrian succession is described in detail by Eganov et al. (1984) and Meert et al. (2011). We focused on the lowermost Kyrshabakty Formation which is part of the Tamdy Series and comprises a ~45 m thick diamictite layer (Aktas tillite) overlain by ~3.5-4 m thick cream-to-ivory-colored cap dolomites without any noticeable sedimentary features besides a fine lamination. Up section, the succession is marked by alternation of dolomitic sandstones and sandy dolostones with an increasing trend in dolomite content towards the top. The first ~30 m of the section are defined by a transgressive system tract and the palaeoenvironment is suggested to represent a very shallow water platform setting which is also confirmed by Eganov et al. (1986).

**Congo craton (Namibia)**

The analyzed marine successions were all situated on the low-latitude (Fig. DR1) continental margin of the southern Congo craton and comprise Neoproterozoic to Cambrian rocks. We concentrate on the thick sequence of carbonate rocks corresponding to the Tsumeb Subgroup, being part of the Otavi Group (Hoffmann et al., 2004; Kaufman et al., 1991). In detail, the shallow-marine platform Ombaatjie and Khowarib Sections as well as the shelf break Fransfontein Section (see Fig. 1 manuscript) provide access to Ghaub glacial deposits (~635

Ma, Hoffmann et al., 2004) overlain by post-glacial Keilberg Member cap dolomites transitioning into a >100 m thick succession of Maieberg Formation dolo- and limestones (Hoffman et al., 1996; Kasemann et al., 2010; Kaufman et al., 1991). The cap carbonates are micritic dolostones, which can be subdivided into a basal laminated unit, a middle unit containing soft-sediment deformation, sheet-cracks and stromatolite structures and a capping interval of thin-bedded dolostones. The Maieberg Formation is comprised of rhythmite limestones and thin-bedded dolo- and limestones at the Khowarib and Ombaatjie Section and only of thin-bedded dolostones at the Fransfontein Section (Kasemann et al., 2010). A more detailed stratigraphy and overview about the large-scale tectonic situation is provided e.g. by Miller (2008).

## SAMPLE SELECTION CRITERIA / ALTERATION EVALUATION

Sample selection and quality evaluation for the Namibian carbonate dataset is described in Kasemann et al. (2010). Fresh rock hand samples of the Kyrshabakty Formation (Kazakhstan) and the Doushantuo Formation (South China) carbonates were taken in 10-30 cm intervals and selected by their uniformity and absence of any obvious alteration or veining. To assure a good sample quality, we checked the samples macroscopically in the field, afterwards microscopically in the lab (thin section, scanning electron microscopy) and performed geochemical tests (trace element and oxygen isotope analyses). Rock powders were prepared from pre-screened, micritic, cleaned and fresh surface rock chips with an agate vibratory disc mill at the Museum für Naturkunde Berlin, Germany.

## METHODS

### Boron measurements

Boron ($\delta^{11}B$) isotope analyses were performed by the method detailed in Kasemann et al. (2001). For analyses, 10 mg of the sample powder was dissolved in 100 µl 1 N HCl for 24 h at

20°C and subsequently centrifuged. The $n(^{11}B)/n(^{10}B)$ measurements were performed on a Thermo Fisher Scientific TRITON *Plus* mass spectrometer, using negative thermal ionization mass spectrometry (N-TIMS). 1 µl boron-free seawater emitter (Vogl et al., 2011) was placed on a degassed Re single filament and dried at 0.7 A. Subsequently, 1 µl of the sample solution containing ~1 ng B was added, evaporated to complete dryness at 0.7 A and afterwards heated at 1.2 A for 30 s. Boron isotopes were registered as $BO_2^-$ complexes on masses 42 and 43, and measurements were carried out at 970°-1050°C with an ion beam intensity of 3-30 pA on mass 43. Each measuring procedure consisted of up to 200 blocks with 10 cycles, taking about 3 hours of data acquisition. To correct for a $CNO^-$ interference on mass 42 occurring at the beginning of some measurements and for isotopic fractionation during analysis, the extrapolation technique described by Kasemann et al. (2001) was used during data evaluation.

Boron isotope ratios are given in $\delta^{11}$B-notation relative to the certified reference material NIST SRM 951 that showed an $^{11}B/^{10}B$ ratio of 4.0068±0.0016 (2sd=0.4‰, n=37 over a period of 12 month). In addition to the NIST material, the standard material M93-TB-FC-1, a *Porites* coral with a published value of 24.8±0.4‰ ($2\sigma_{mean}$), as determined by different multicollector techniques (Kasemann et al., 2009), was also regularly analyzed. The coral replicates gave $\delta^{11}B$ of 24.1±0.7‰ (2sd, n=16). Samples were analyzed at least twice and their reproducibility (2sd) is given in Table DR1.

**Carbon and oxygen measurements**

The $\delta^{13}C_{carb}$ and $\delta^{18}O$ isotope dataset is based on 14 bulk rock samples of the Kyrshabakty Section and 9 samples of the Xiaofenghe Section, respectively. All measurements were carried out on a Thermo Finnigan GASBENCH II linked online to a Thermo Finnigan DELTA V isotope ratio mass spectrometer at the Museum fuer Naturkunde Berlin, Germany. Isotope ratios are reported in δ-notation in [‰] relative to the Vienna Peedee Belemnite (VPDB). The analytical reproducibility of $\delta^{13}C_{carb}$ and $\delta^{18}O$ values is each generally better than ±0.2‰ (2sd).

## Trace element analyses

Trace elements analyses (Table DR2) of the northern Xiaofenghe Section carbonates were performed on an Agilent Technologies 700 Series ICP-OES at the inorganic geochemistry group of the MARUM, Germany. Three replicates of each dilution/concentration were measured and typically had a relative standard deviation (RSD) of better than 3% (excepting boron, which was < 7%).

## Clay contamination

To avoid contamination by the dissolution of boron-bearing clays during chemical preparation a 1N HCl (100 µl 1 N HCl for 10mg of sample powder) is used during the dissolution procedure. Dissolution of B-bearing clays would generally increase the boron concentration. Potential modification of the isotope composition is dependent on the clay source and hence difficult to assess, but is expected to be negligible due to a similar fractionation factor between seawater - carbonates and seawater - clay (Palmer et al., 1987). To assess the amount of clay in the sample material XRD analyses of Kyrshabakty Formation cap dolomites were performed at the Mineralogy Department of the Technical University Berlin, Germany. A semi-quantitative data evaluation after Cook et al. (1975) showed an average clay content <1%. XRD analyses of the Chinese data set done at the ZEKAM, University of Bremen, Germany showed average clay content of ~6%. To test for clay contamination in the sample solution, trace element analyses were performed on an Agilent Technologies 700 Series ICP-OES at the inorganic geochemistry group, University of Bremen, Germany. The boron concentration is 2 µg $g^{-1}$ without any obvious correlation to varying clay content. For example, Al concentrations are around 200 ppm (Table DR2) and are not correlated to the B concentration ($R^2$=0.22). In addition, there is no correlation of boron concentration and boron isotope values at the 95% significance level ($R^2$=0.46). Hence boron contamination by clay dissolution can be excluded.

## Post-depositional alteration

Post-depositional alteration, especially diagenesis, is thought to decrease the isotopic composition of oxygen, boron and carbon isotopes (Derry et al., 1992; Kaufman et al., 1993; Paris et al., 2010; Veizer et al., 1999). On that account, only samples with $\delta^{18}O$ values > -10‰ are considered to be of primary origin and suitable for further isotope analyses. Doushantuo Formation dolomites show average $\delta^{18}O$ values of -6.8‰ with no $\delta^{18}O$ value lower than -7.3‰ and without any significant correlation at the 5% significance level ($R^2$=0.22) to the carbon (Fig. DR2) or boron isotopic composition. A similar situation holds with respect to the Kyrshabakty Formation data. The average $\delta^{18}O$ value is -5‰ and as per the Chinese data there is no significant or obvious correlation with $\delta^{13}C$ at the 5% significance level ($R^2$=0.07, Fig. DR2) or with $\delta^{11}B$ data. Further, both the $\delta^{18}O$ and $\delta^{13}C$ are in perfect agreement with literature data for that time (e.g. Jacobsen and Kaufman, 1999). Diagenesis is also thought to cause a correlation between the boron concentration and the $\delta^{11}B$ values (Spivack and You, 1997). However, no relationship is obvious for our data set.

For the Phanerozoic, primary isotopic signals recorded by carbonates are expected to show Mn/Sr ratios below 10. In comparison, Mn/Sr values above 10 are present in China, which could be a result of hydrothermal overprint, as suggested for the Doushantuo Formation (Derkowski et al., 2013). However, enriched Mn/Sr are a common feature of cap dolomites and also reported by e.g. Liu et al. (2013). In general, the reliability of Mn/Sr ratios as an alteration criterion is doubted for Neoproterozoic rocks by many authors. This is due to its being strongly dependent on the primary precipitated carbonate mineral phase (Derry, 2010), and high Mn/Sr ratios can also result from precipitation in early diagenetic anoxic waters (Miller et al., 2009), potentially present during the time of cap dolomite deposition. Also, increased seawater concentrations of Mn and Fe (see Table DR2) leading to high Mn/Sr during the Marinoan time interval are likely, due to the potential absence of abundant oxygen and sulfate necessary for redox reactions

(Anbar and Knoll, 2002; Hoffman and Li, 2009; Miller et al., 2009; Raub et al., 2007). We therefore conclude that our boron isotope data have not been diagenetically compromised. In addition, systematic cyclical isotopic patterns at all measured sections and on different continents further supports interpreting the isotopic signatures as primary values.

## CONSTRAINTS ON OCEAN pH RECONSTRUCTION

In seawater two dominant boron species are present: boric acid ($B(OH)_3$) and borate-ion ($B(OH)_4^-$) (Kakihana et al., 1977; Spivack and Edmond, 1987). Between these two species an isotopic exchange (Hemming and Hanson, 1992) is described by the reaction displayed in equation [1]:

$$^{11}B(OH)_3 + {}^{10}B(OH)_4^- <=> {}^{10}B(OH)_3 + {}^{11}B(OH)_4^- \quad [1]$$

Due to the fact that the abundance of the species and their isotopic composition is pH dependent and marine carbonates predominantly incorporate the charged, tetrahedral species (Hemming and Hanson, 1992; Sanyal et al., 2000), palaeo pH calculations by boron isotope measurements are possible (Klochko et al., 2006), with the relationship given in equation [2]:

$$pH = pK_B - \log\left[ - \frac{\delta^{11}B_{SW} - \delta^{11}B_{carb}}{\delta^{11}B_{SW} - \alpha_{B3\text{-}B4} \cdot \delta^{11}B_{carb} - 1000 \cdot (\alpha_{B3\text{-}B4} - 1)} \right] \quad [2]$$

To calculate seawater pH, we need the B isotope composition of the carbonate ($\delta^{11}B_{carb}$) and the seawater ($\delta^{11}B_{sw}$) (discussed below), as well as the isotope fractionation factor for boron ($\alpha_{B3\text{-}B4}$) and the dissociation constant of boric acid ($pK_B$), both of which are temperature dependent. To infer ocean pH values and compare the pH patterns of the different continents, we performed ocean pH calculations with a $\delta^{11}B_{sw}$ value of 20.5‰ (see below) using the empirical fractionation factor for seawater pH and the B isotopic compositions of borate in solution and carbonates of $\alpha_{B3\text{-}B4} = 1.0272$ (Klochko et al., 2006), and a $pK_B$ of 8.579 (Dickson, 1990) both for 25°C seawater temperature. Since exact seawater temperatures for the Early

169 Ediacaran are unknown we have to rely on modelled values. Initial seawater temperatures
170 of -1.5°C rapidly increasing to ~30°C after the deglacial are modelled by Higgins and Schrag
171 (2003). Variations in sea surface temperatures between 15°C and 35°C, most likely reflecting
172 the temperatures prevailing during platform carbonate precipitation, would result in a maximum
173 difference of < 0.2 pH. Generally, colder temperatures lead to slightly higher pH conditions,
174 whereas warmer seawater temperatures lead to slightly more acidic conditions. For our dataset,
175 the relative ocean pH pattern including the acidification magnitudes would stay completely the
176 same.

177 The $pK_B$ also changes with different salinities (Dickson, 1990). However, even if lower
178 salinities (S= ~25 ppt) are assumed due to meltwater influx (Shields, 2005) the associated
179 isotopic variations are negligible for our dataset and a salinity assumption of S = 35 ppt is used
180 for calculations.

181 Modern seawater is taken as homogeneous with a $\delta^{11}B_{sw}$ of 39.6‰ (e.g. Foster et al., 2010). In
182 the past, significant variations in $\delta^{11}B_{sw}$ are likely and attributed to changes in the global boron
183 budget (Joachimski et al., 2005). The residence time of boron in the modern ocean is ~14-20
184 Ma (Lemarchand et al., 2000; Spivack, 1986) and should be roughly similar during the
185 Neoproterozoic, but is in any case far higher than the maximal assumed duration of cap
186 carbonate deposition (~3 Ma, Condon et al., 2005). Consequently, ocean-pH changes instead
187 of variations in seawater $\delta^{11}B$ composition are recorded at the investigated sections. To gauge
188 ocean pH conditions in the Neoproterozoic, Kasemann et al. (2005) initially explored different
189 pH profiles with basic and acidic end-members. Subsequently, Kasemann et al. (2010) opted
190 for slightly acidic seawater conditions, based on pH models for the Precambrian (Grotzinger
191 and Kasting, 1993; Higgins and Schrag, 2003) and calculated relative ocean pH variation of as
192 much as 1.5 pH units based on $\delta^{11}B_{sw}$ values between 20‰ and 23‰. By combining our new
193 Chinese and Kazakh dataset together with the already published Namibian literature data, we

suggest and use a seawater composition of 20.5‰ as our 'best-guess' value. Using a higher isotope composition for the seawater, unlikely acidic conditions (< pH 6) for the acidification event would result for some sections, while assumed lower $\delta^{11}B_{sw}$ would lead to highly alkaline seawater conditions (> pH 9.5). In comparison to models and calculations for that time (e.g. Higgins and Schrag, 2003; Kempe and Kazmierczak, 2002), we regard each as unlikely. For a better comparison and overview, we nevertheless performed ocean pH calculations for different $\delta^{11}B$ seawater assumptions (A: 20.5‰, B: 21.5‰, and C: 22.5‰) summarized in Table DR1. The overall acidification pattern observed at all sections is only negligibly affected by changes to the boron isotope seawater composition. For the Ombaatjie Section a pH calculation is only possible with model A, due to its very low boron isotope ratios (note that the uncertainty of the isotope value is ~1‰ ($2\sigma_f$) for the Ombaatjie Section).

We evaluate the observed initial and maximum differences in seawater pH (~1 pH unit) between the investigated sections as reasonable, especially in respect of modern large-scale open ocean surface water pH measurements showing variation >0.5 pH (Doney, 2006; Takahashi et al., 2014). Even larger differences must be expected on local to regional scale and ocean pH in fact differs on a daily and monthly basis (Hofmann et al., 2011). Additionally, local and regional differences in seawater pH between different sample localities can result from e.g. upwelling, riverine influx, productivity regimes and alkalinity states (Kisakurek et al., 2005; Pearson and Palmer, 2000; Takahashi et al., 2014).

## ALTERNATIVE MODELS FOR A POSTGLACIAL ALKALINE OCEAN AND A SUBSEQUENT OCEAN ACIDIFICATION

As mentioned in the manuscript, different explanations may exist for alkaline ocean pH condition at the onset of cap carbonate deposition. Apart from assuming a global ice shield preventing air-sea gas exchange during glaciation, a continental weathering pulse at the beginning of deglaciation (Le Hir et al., 2009) and/or the development of a meltwater plume

(Shields, 2005) could each serve as reasons. Highly reactive and quickly dissolving glacial rock flour (Le Hir et al., 2009) produced during continuous grinding of continental surfaces by ice sheet dynamics could have been washed into the ocean causing an intense weathering pulse that might have buffered the seawater immediately after the glaciation and caused alkaline seawater conditions and high $\delta^{11}B$ values at the start of cap carbonate deposition. To assess the potential influx and buffering capacity of glacial rock flour, additional proxy data that respond to weathering over short timescales are needed. Alternatively, sea-ice and glacial meltwater injected into the ocean could have led to the evolution of a widespread meltwater plume and could have affected the pH of the surface ocean. Recent studies on meltwater demonstrate a highly variable $CO_2$-carbonate chemistry together with significant differences in pH values of meltwater from ~5 to >10 including supraglacial and subglacial meltwater drainage, glacial rivers, melt ponds, deposited snow, brines and sea ice (Bates et al., 2014; e.g. Hare et al., 2013; Larose et al., 2010; Singh et al., 2012; Tegt, 2002). These tremendous differences in pH are controlled by e.g. $CO_2$ uptake from the atmosphere, sea ice freezing processes, host rock compositions below the glaciers and varying chemical weathering rates (Wimpenny et al., 2010) and make it difficult to predict the balance and dynamics of ocean pH in today's high latitude world (Bates et al., 2014), and to even assess the pH influence of meltwater influx into the postglacial Ediacaran ocean. In a recent study, Feely and Kleypas (2012) performed a mass-balance modeling of a situation involving melting of the Arctic and Antarctic ice caps, probably the best approximate to the post-Marinoan meltwater plume hypothesis described by e.g. Liu et al. (2014) and Shields (2005). They suggest an initial increase in seawater pH due to the enormous dilution effect of the meltwater with respect to e.g. salinity, alkalinity, and carbon content, which could comply with the observed alkaline pH observed for the onset of cap carbonate deposition. The resulting $pCO_2$ disequilibrium between seawater and atmosphere causes enhanced oceanic $CO_2$ uptake inducing an ocean acidification. Again this could be comparable to the observed transition pattern into ocean

acidification during cap carbonate deposition in the Marinoan aftermath. $CO_2$ uptake would continue until the ocean reaches equilibrium and ocean acidification would be sustained until the climate is regulated by $CO_2$ draw down.

## ISOCHRONOUS VS DIACHRONOUS CAP CARBONATE DEPOSITION

Hoffman et al. (2007) argue that sedimentary structures as well as the carbon isotope record from the platform to the lower slope in Namibia support a diachronous deposition of post-glacial cap carbonates. This is based on the observation that the overall sigmoidal trajectory of the carbon isotope signal is only incompletely sampled in any single section. If so, then the boron isotope signal should reveal similar incomplete sigmoidal trajectories across the basin. This is, however, not the case since our data show rather complete and synchronous pattern. In view of a potential meltwater plume after deglaciation, the B isotope profiles would fit the semi-diachronous model promoted by Shields (2005). Initially, cap dolostones, in our case the basal laminated Keilberg dolostone, are deposited under the, for example, influence of an incipient meltwater plume above the deeper water setting. As the plume grows it floods the bank such that the interval of ocean acidification is then largely captured within the upper Keilberg dolostone deposits. By the time of Maieberg limestone deposition, the pH of the seawater on the platform is buffered by local changes in alkalinity i.e. continental weathering. This scenario is compatible with the conditions hypothesized by Shields (2005). An isochronous or semi-diachronous model for cap dolomite deposition is also suggested for additional palaeo-continents: Mongolia and South Australia (Liu et al., 2014).

While our boron isotope record from the platform to the lower slope supports a synchronous or semi-diachronous cap carbonate deposition model, we nevertheless cannot completely rule out the possibility of a diachronous model.

## REFERENCES


Alexeiev, D. V., Cook, H. E., Buvtyshkin, V. M., and Golub, L. Y., 2009, Structural evolution of the Ural-Tian Shan junction: A view from Karatau ridge, South Kazakhstan: Comptes Rendus Geosciences, v. 341, no. 2-3, p. 287-297.

Allen, M. B., Alsop, G. I., and Zhemchuzhnikov, V. G., 2001, Dome and basin refolding and transpressive inversion along the Karatau Fault System, southern Kazakstan: Journal of the Geological Society, v. 158, no. 1, p. 83-95.

Anbar, A. D., and Knoll, A. H., 2002, Proterozoic Ocean Chemistry and Evolution: A Bioinorganic Bridge?: Science, v. 297, no. 5584, p. 1137-1142.

Bates, N. R., Garley, R., Frey, K. E., Shake, K. L., and Mathis, J. T., 2014, Sea-ice melt CO2-carbonate chemistry in the western Arctic Ocean: meltwater contributions to air-sea CO2 gas exchange, mixed layer properties and rates of net community production under sea ice: Biogeosciences Discuss., v. 11, no. 1, p. 1097-1145.

Condon, D., Zhu, M., Bowring, S., Wang, W., Yang, A., and Jin, Y., 2005, U-Pb Ages from the Neoproterozoic Doushantuo Formation, China: Science, v. 308, no. 5718, p. 95-98.

Cook, H. E., Johnson, P. D., Matti, J. C., and Zemmels, I., 1975, Methods of sample preparation and X-ray diffraction data analysis, X-ray Mineralogy Laboratory, Deep Sea Drilling Project, University of California, Riverside: In: Hayes, D.E., Frakes, L.A., et al., Init. Repts.

Derkowski, A., Bristow, T. F., Wampler, J. M., Środoń, J., Marynowski, L., Elliott, W. C., and Chamberlain, C. P., 2013, Hydrothermal alteration of the Ediacaran Doushantuo Formation in the Yangtze Gorges area (South China): Geochimica et Cosmochimica Acta, v. 107, no. 0, p. 279-298.

Derry, L. A., 2010, A burial diagenesis origin for the Ediacaran Shuram–Wonoka carbon isotope anomaly: Earth and Planetary Science Letters, v. 294, no. 1-2, p. 152-162.

Derry, L. A., Kaufman, A. J., and Jacobsen, S. B., 1992, Sedimentary cycling and environmental change in the Late Proterozoic: Evidence from stable and radiogenic isotopes: Geochimica et Cosmochimica Acta, v. 56, no. 3, p. 1317-1329.

296 Dickson, A. G., 1990, Thermodynamics of the dissociation of boric acid in synthetic seawater from
297 273.15 to 318.15 K: Deep Sea Research Part A. Oceanographic Research Papers, v. 37, no. 5,
298 p. 755-766.
299 Doney, S. C., 2006, The Dangers of Ocean Acidification: Scientific American, v. 294, p. 58-65.
300 Eganov, E. A., Ergaliev, G. K., Ilyin, A. V., and Krasnov, A. A., 1984, Guidebook / International
301 Geological Congress, XXVII Session Kazakhstan: Karatau Phosphorite Basin, Moskau,
302 Nauka.
303 Eganov, E. A., Sovetov, Y. K., and Yanshin, A. L., 1986, Proterozoic and Cambrian phosphorite
304 deposits: Karatau, southern Kazakhstan, USSR: In: Cook, P.J., Shergold, J.H. (Eds.),
305 Phosphate Deposits of the World: Volume 1 Proterozoic and Cambrian Phosphorites.
306 Cambridge University Press, Cambridge, UK, p. 175-189.
307 Feely, R. A., and Kleypas, J., 2012, *in* Cooley, S., Mathis, J., Yates, K., Turley, C., Frequently Asked
308 Questions about Ocean Acidification, ed.: U.S. Ocean Carbon and Biogeochemistry Program
309 and the UK Ocean Acidification Research Programme, Version 2, www.whoi.edu/OCB-
310 OA/FAQs.
311 Foster, G. L., Pogge von Strandmann, P. A. E., and Rae, J. W. B., 2010, Boron and magnesium
312 isotopic composition of seawater: Geochemistry, Geophysics, Geosystems, v. 11.
313 Grotzinger, J. P., and Kasting, J. F., 1993, New Constraints on Precambrian Ocean Composition: The
314 Journal of Geology, v. 101, no. 2, p. 235-243.
315 Hare, A. A., Wang, F., Barber, D., Geilfus, N. X., Galley, R. J., and Rysgaard, S., 2013, pH evolution
316 in sea ice grown at an outdoor experimental facility: Marine Chemistry, v. 154, p. 46-54.
317 Hemming, N. G., and Hanson, G. N., 1992, Boron isotopic composition and concentration in modern
318 marine carbonates: Geochimica et Cosmochimica Acta, v. 56, no. 1, p. 537-543.
319 Higgins, J. A., and Schrag, D. P., 2003, Aftermath of a snowball Earth: Geochemistry, Geophysics,
320 Geosystems, v. 4, no. 3, p. 1028.
321 Hoffman, P. F., Halverson, G. P., Domack, E. W., Husson, J. M., Higgins, J. A., and Schrag, D. P.,
322 2007, Are basal Ediacaran (635 Ma) post-glacial “cap dolostones” diachronous?: Earth and
323 Planetary Science Letters, v. 258, no. 1–2, p. 114-131.

Hoffman, P. F., Hawkins, D. P., Isachsen, C. E., and Bowring, S. A., 1996, Precise U-Pb zircon ages for early Damaran magmatism in the Summas Mountains and Welwitschia Inlier, northern Damara Belt, Namibia: Communications of the Geological Survey of Namibia, v. 11, p. 47-52.

Hoffman, P. F., and Li, Z.-X., 2009, A palaeogeographic context for Neoproterozoic glaciation: Palaeogeography, Palaeoclimatology, Palaeoecology, v. 277, no. 3–4, p. 158-172.

Hoffmann, K.-H., Condon, D. J., Bowring, S. A., and Crowley, J. L., 2004, U-Pb zircon date from the Neoproterozoic Ghaub Formation, Namibia: Constraints on Marinoan glaciation: Geology, v. 32, no. 9, p. 817-820.

Hofmann, G. E., Smith, J. E., Johnson, K. S., Send, U., Levin, L. A., Micheli, F., Paytan, A., Price, N. N., Peterson, B., Takeshita, Y., Matson, P. G., Crook, E. D., Kroeker, K. J., Gambi, M. C., Rivest, E. B., Frieder, C. A., Yu, P. C., and Martz, T. R., 2011, High-Frequency Dynamics of Ocean pH: A Multi-Ecosystem Comparison: Plos One, v. 6, no. 12.

Jacobsen, S. B., and Kaufman, A. J., 1999, The Sr, C and O isotopic evolution of Neoproterozoic seawater: Chemical Geology, v. 161, no. 1–3, p. 37-57.

Jiang, G., Kennedy, M. J., and Christie-Blick, N., 2003, Stable isotopic evidence for methane seeps in Neoproterozoic postglacial cap carbonates: Nature, v. 426, no. 6968, p. 822-826.

Joachimski, M. M., Simon, L., van Geldern, R., and Lécuyer, C., 2005, Boron isotope geochemistry of Paleozoic brachiopod calcite: Implications for a secular change in the boron isotope geochemistry of seawater over the Phanerozoic: Geochimica et Cosmochimica Acta, v. 69, no. 16, p. 4035-4044.

Kakihana, H., Kotaka, M., Satoh, S., Nomura, M., and Okamoto, M., 1977, Fundamental Studies on the Ion-Exchange Separation of Boron Isotopes: Bulletin of the Chemical Society of Japan, v. 50, no. 1, p. pp.158-163.

Kasemann, S. A., Hawkesworth, C. J., Prave, A. R., Fallick, A. E., and Pearson, P. N., 2005, Boron and calcium isotope composition in Neoproterozoic carbonate rocks from Namibia: evidence for extreme environmental change: Earth and Planetary Science Letters, v. 231, no. 1-2, p. 73-86.

352 Kasemann, S. A., Meixner, A., Rocholl, A., Vennemann, T., Rosner, M., Schmitt, A. K., and
353 Wiedenbeck, M., 2001, Boron and Oxygen Isotope Composition of Certified Reference
354 Materials NIST SRM 610/612 and Reference Materials JB-2 and JR-2: Geostandards
355 Newsletter, v. 25, no. 2-3, p. 405-416.
356 Kasemann, S. A., Prave, A. R., Fallick, A. E., Hawkesworth, C. J., and Hoffmann, K.-H., 2010,
357 Neoproterozoic ice ages, boron isotopes, and ocean acidification: Implications for a snowball
358 Earth: Geology, v. 38, no. 9, p. 775-778.
359 Kasemann, S. A., Schmidt, D. N., Bijma, J., and Foster, G. L., 2009, In situ boron isotope analysis in
360 marine carbonates and its application for foraminifera and palaeo-pH: Chemical Geology, v.
361 260, no. 1-2, p. 138-147.
362 Kaufman, A. J., Hayes, J. M., Knoll, A. H., and Germs, G. J. B., 1991, Isotopic composition of
363 carbonates and organic-carbon from upper Proterozoic successions in Namibia - Stratigraphic
364 variation and the effects of diagenesis and metamorphism: Precambrian Research, v. 49, no. 3-
365 4, p. 301-327.
366 Kaufman, A. J., Jacobsen, S. B., and Knoll, A. H., 1993, The Vendian record of Sr and C isotopic
367 variations in seawater: Implications for tectonics and paleoclimate: Earth and Planetary
368 Science Letters, v. 120, no. 3–4, p. 409-430.
369 Kempe, S., and Kazmierczak, J., 2002, Biogenesis and Early Life on Earth and Europa: Favored by an
370 Alkaline Ocean?: Astrobiology, v. 2, no. 1, p. 123-130.
371 Kisakurek, B., James, R. H., and Harris, N. B. W., 2005, Li and [delta]7Li in Himalayan rivers:
372 Proxies for silicate weathering?: Earth and Planetary Science Letters, v. 237, no. 3-4, p. 387-
373 401.
374 Klochko, K., Kaufman, A. J., Yao, W., Byrne, R. H., and Tossell, J. A., 2006, Experimental
375 measurement of boron isotope fractionation in seawater: Earth and Planetary Science Letters,
376 v. 248, no. 1-2, p. 276-285.
377 Larose, C., Dommergue, A., De Angelis, M., Cossa, D., Averty, B., Marusczak, N., Soumis, N.,
378 Schneider, D., and Ferrari, C., 2010, Springtime changes in snow chemistry lead to new

379 insights into mercury methylation in the Arctic: Geochimica et Cosmochimica Acta, v. 74, no.
380 22, p. 6263-6275.
381 Le Hir, G., Donnadieu, Y., Goddéris, Y., Pierrehumbert, R. T., Halverson, G. P., Macouin, M.,
382 Nédélec, A., and Ramstein, G., 2009, The snowball Earth aftermath: Exploring the limits of
383 continental weathering processes: Earth and Planetary Science Letters, v. 277, no. 3–4, p. 453-
384 463.
385 Lemarchand, D., Gaillardet, J., Lewin, E., and Allegre, C. J., 2000, The influence of rivers on marine
386 boron isotopes and implications for reconstructing past ocean pH: Nature, v. 408, no. 6815, p.
387 951-954.
388 Li, Z.-X., Evans, D. A. D., and Halverson, G. P., 2013, Neoproterozoic glaciations in a revised global
389 palaeogeography from the breakup of Rodinia to the assembly of Gondwanaland: Sedimentary
390 Geology, v. 294, no. 0, p. 219-232.
391 Liu, C., Wang, Z., and Raub, T. D., 2013, Geochemical constraints on the origin of Marinoan cap
392 dolostones from Nuccaleena Formation, South Australia: Chemical Geology, v. 351, no. 0, p.
393 95-104.
394 Liu, C., Wang, Z., Raub, T. D., Macdonald, F. A., and Evans, D. A. D., 2014, Neoproterozoic cap-
395 dolostone deposition in stratified glacial meltwater plume: Earth and Planetary Science
396 Letters, v. 404, no. 0, p. 22-32.
397 Ma, G., Li, H., and Zhang, Z., 1984, An investigation of the age limits of the Sinian System in South
398 China: Bulletin of Yichang Institute of Geology Mineral Resources, v. 8, p. 1-29.
399 Meert, J. G., Gibsher, A. S., Levashova, N. M., Grice, W. C., Kamenov, G. D., and Ryabinin, A. B.,
400 2011, Glaciation and ~ 770 Ma Ediacara (?) Fossils from the Lesser Karatau Microcontinent,
401 Kazakhstan: Gondwana Research, v. 19, no. 4, p. 867-880.
402 Miller, N. R., Stern, R. J., Avigad, D., Beyth, M., and Schilman, B., 2009, Cryogenian slate-carbonate
403 sequences of the Tambien Group, Northern Ethiopia (I): Pre-“Sturtian” chemostratigraphy and
404 regional correlations: Precambrian Research, v. 170, no. 3–4, p. 129-156.
405 Miller, R. M., 2008, The geology of Namibia: Palaeozoic to Cenozoic, Windhoek, Geological Survey,
406 Namibia.

Palmer, M. R., Spivack, A. J., and Edmond, J. M., 1987, Temperature and pH controls over isotopic fractionation during adsorption of boron on marine clay: Geochimica et Cosmochimica Acta, v. 51, no. 9, p. 2319-2323.

Paris, G., Bartolini, A., Donnadieu, Y., Beaumont, V., and Gaillardet, J., 2010, Investigating boron isotopes in a middle Jurassic micritic sequence: Primary vs. diagenetic signal: Chemical Geology, v. 275, no. 3-4, p. 117-126.

Pearson, P. N., and Palmer, M. R., 2000, Atmospheric carbon dioxide concentrations over the past 60 million years: Nature, v. 406, no. 6797, p. 695-699.

Raub, T. D., Evans, D. A. D., and Smirnov, A. V., 2007, Siliciclastic prelude to Elatina–Nuccaleena deglaciation: lithostratigraphy and rock magnetism of the base of the Ediacaran system: Geological Society, London, Special Publications, v. 286, no. 1, p. 53-76.

Sanyal, A., Nugent, M., Reeder, R. J., and Bijma, J., 2000, Seawater pH control on the boron isotopic composition of calcite: evidence from inorganic calcite precipitation experiments: Geochimica et Cosmochimica Acta, v. 64, no. 9, p. 1551-1555.

Shields, G. A., 2005, Neoproterozoic cap carbonates: a critical appraisal of existing models and the plumeworld hypothesis: Terra Nova, v. 17, no. 4, p. 299-310.

Singh, V., Ramanathan, A. L., Pottakkal, J., Sharma, P., Linda, A., Azam, M., and Chatterjee, C., 2012, Chemical characterisation of meltwater draining from Gangotri Glacier, Garhwal Himalaya, India: Journal of Earth System Science, v. 121, no. 3, p. 625-636.

Spivack, A. J., 1986, Boron isotope geochemistry [Ph.D.: Massachusetts Institute of Technology], 184 p.

Spivack, A. J., and Edmond, J. M., 1987, Boron isotope exchange between seawater and the oceanic crust: Geochimica et Cosmochimica Acta, v. 51, no. 5, p. 1033-1043.

Spivack, A. J., and You, C.-F., 1997, Boron isotopic geochemistry of carbonates and pore waters, Ocean Drilling Program Site 851: Earth and Planetary Science Letters, v. 152, no. 1–4, p. 113-122.

Takahashi, T., Sutherland, S. C., Chipman, D. W., Goddard, J. G., Ho, C., Newberger, T., Sweeney, C., and Munro, D. R., 2014, Climatological distributions of pH, pCO2, total CO2, alkalinity,

and CaCO3 saturation in the global surface ocean, and temporal changes at selected locations: Marine Chemistry, v. 164, no. 0, p. 95-125.

Tegt, S. K., 2002, The chemical evolution of Canada glacier melt: Supraglacial and proglacial waters in Taylor Valley Antartica [M.S.: The Ohio State University, 149 p.

Veizer, J., Ala, D., Azmy, K., Bruckschen, P., Buhl, D., Bruhn, F., Carden, G. A. F., Diener, A., Ebneth, S., Godderis, Y., Jasper, T., Korte, C., Pawellek, F., Podlaha, O. G., and Strauss, H., 1999, 87Sr/86Sr, δ13C and δ18O evolution of Phanerozoic seawater: Chemical Geology, v. 161, no. 1–3, p. 59-88.

Vogl, J., Rosner, M., and Pritzkow, W., 2011, Development and validation of a single collector SF-ICPMS procedure for the determination of boron isotope ratios in water and food samples: Journal of Analytical Atomic Spectrometry, v. 26, no. 4, p. 861-869.

Wimpenny, J., James, R. H., Burton, K. W., Gannoun, A., Mokadem, F., and Gíslason, S. R., 2010, Glacial effects on weathering processes: New insights from the elemental and lithium isotopic composition of West Greenland rivers: Earth and Planetary Science Letters, v. 290, no. 3–4, p. 427-437.

Xiao, S., McFadden, K. A., Peek, S., Kaufman, A. J., Zhou, C., Jiang, G., and Hu, J., 2012, Integrated chemostratigraphy of the Doushantuo Formation at the northern Xiaofenghe section (Yangtze Gorges, South China) and its implication for Ediacaran stratigraphic correlation and ocean redox models: Precambrian Research, v. 192-195, no. 0, p. 125-141.

Zhang, J. M., Li, G., Zhou, C. M., Zhu, M. Y., and Yu, Z., 1997, Carbon isotope profiles and their correlation across the Neoproterozoic-Cambrian boundary interval on the Yangtze Platform, China: Bulletin of National Museum of Natural Science, v. 10, p. 107-116.

Zhu, M. Y., Zhang, J., Steiner, M., Yang, A., Li, G., and Erdtmann, B.-D., 2003, Sinian-Cambrian stratigraphic framework for shallow-to-deep-water environments of the Yangtze Platform: an integrated approach: Progress in Natural Science, v. 13, no. 12, p. 951-960.

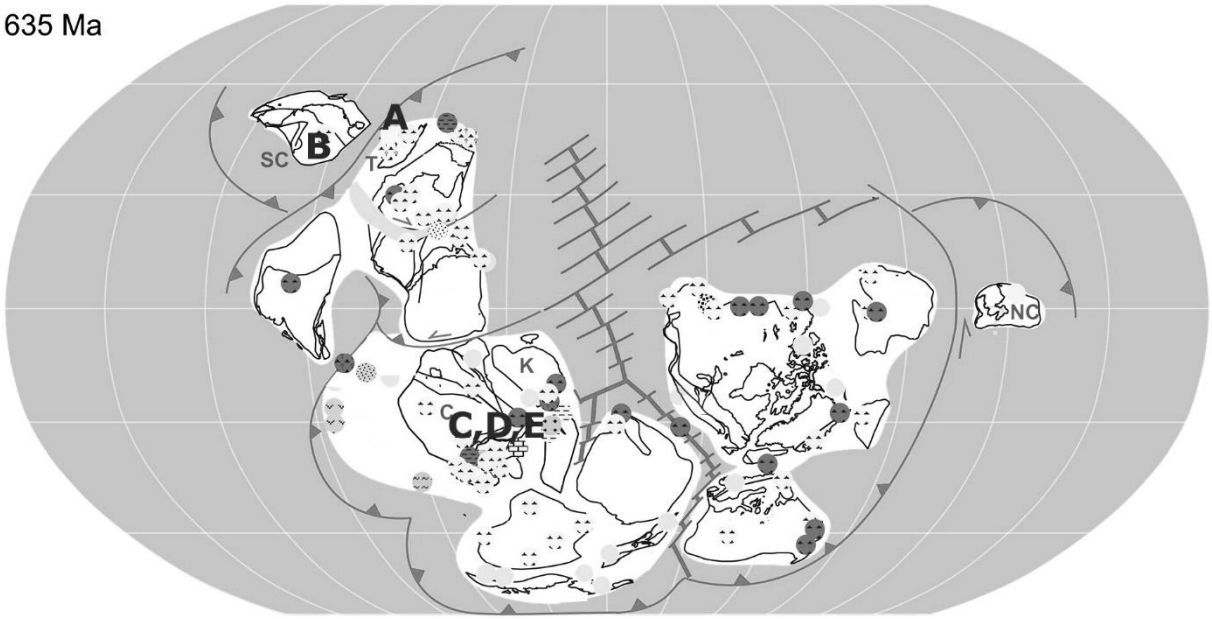


461

462 **Figure DR1:** Palaeogeographic reconstruction for 635 Ma (slightly modified from Li et al.,
463 2013). The investigated sections are indicated in black: A: Kyrshabakty Section, Karatau
464 microcontinent. B: N Xiaofenghe Section, South China Block. C: Ombaatjie Section, Congo
465 craton. D: Khowarib Section, Congo craton. E: Fransfontein Section, Congo craton. The
466 geographic position of the Karatau-Naryn terrane is suggested to be close to South China and
467 the Tarim microcontinent. Abbreviations of the terranes: C-Congo; K-Kalahari; NC-North
468 China; SC-South China; T-Tarim.

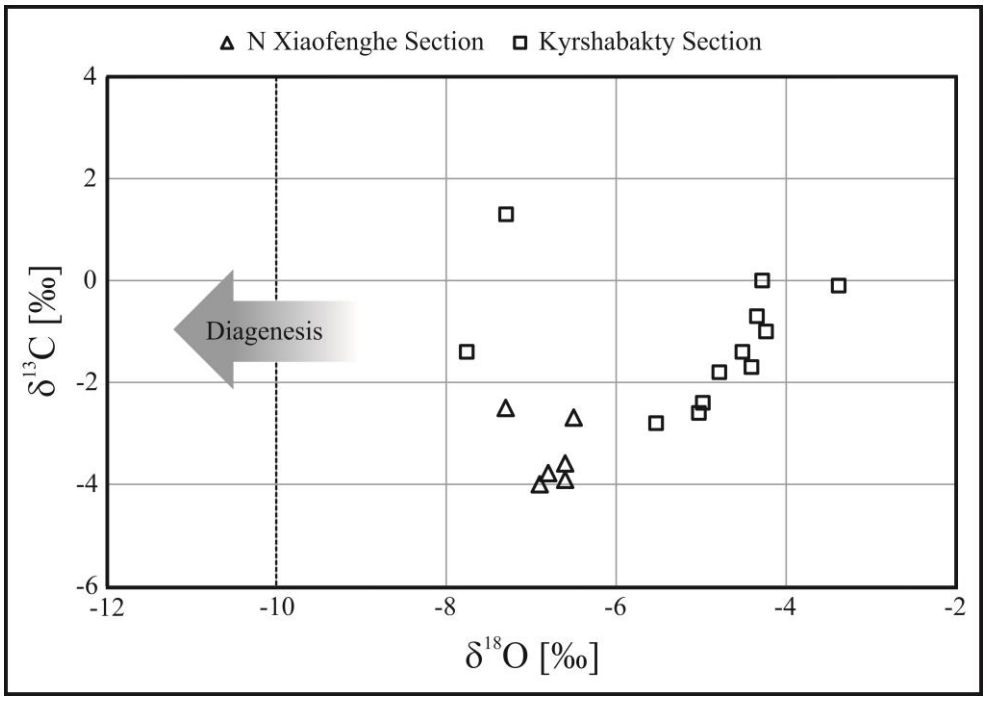


**Figure DR2:** Cross-plot of $\delta^{13}C_{carb}$ vs. $\delta^{18}O$ data of the Northern Xiaofenghe (triangles) and Kyrshabakty Section (squares). No data are in the diagenesis-field and no significant correlation is obvious.

**Assumptions for pH calculations:** $pK_B$ = **8.579** **Dickson, 1990**

$\alpha$ = **1.0272** **Klochko *et al.*, 2006**

**A: 20.5‰** $\delta^{11}B_{seawater}$

**B: 21.5‰** $\delta^{11}B_{seawater}$

**C: 22.5‰** $\delta^{11}B_{seawater}$

| **China** | **Yangtze Platform** | | | | | | | |
|---|---|---|---|---|---|---|---|---|
| **N. Xiaofenghe Section** | | $\delta^{13}C$ | $\delta^{18}O$ | $\delta^{11}B$ | | A | B | C |
| Sample | meter | [‰] | [‰] | [‰] | 2σ | pH | pH | pH |
| NXF0.2 | 0.2 | -4.0 | -6.9 | 9.6 | 0.1 | 8.8 | 8.7 | 8.6 |
| NXF0.75 | 0.8 | -3.6 | -6.6 | 6.8 | 1.3 | 8.6 | 8.5 | 8.5 |
| NXF1.6 | 1.6 | -3.8 | -6.8 | -2.2 | 1.6 | 7.9 | 7.8 | 7.6 |
| NXF2.35B | 2.4 | -3.9 | -6.6 | 4.8 | 0.2 | 8.5 | 8.4 | 8.3 |
| NXF3.85 | 3.9 | -2.7 | -6.5 | 5.4 | 0.0 | 8.5 | 8.4 | 8.4 |
| NXF4.8 | 4.8 | -2.5 | -7.3 | 13.5 | 1.1 | 9.1 | 9.0 | 8.9 |
| NXF6.65 | 6.7 | -0.2 | n.a. | 14.8 | 0.1 | 9.2 | 9.1 | 9.0 |
| NXF22 | 22.0 | 1.8 | n.a. | n.a. | | | | |
| **Kazakhstan** | **Malyi Karatau Range** | | | | | | | |
| **Kyrshabakty Section** | | $\delta^{13}C$ | $\delta^{18}O$ | $\delta^{11}B$ | | A | B | C |
| Sample | meter | [‰] | [‰] | [‰] | 2σ | pH | pH | pH |
| KY 3 | 0.0 | -0.1 | -3.4 | 8.7 | 0.2 | 8.7 | 8.7 | 8.6 |
| KY 4 | 0.2 | -0.7 | -4.3 | 6.5 | 1.2 | 8.6 | 8.5 | 8.4 |
| KY 5a | 0.4 | -1.4 | -4.5 | 6.5 | 1.6 | 8.6 | 8.5 | 8.4 |
| KY 5b | 0.5 | -1.8 | -4.8 | 8.2 | 0.2 | 8.7 | 8.6 | 8.6 |
| KY 6a | 0.8 | n.a. | n.a. | 6.1 | 1.0 | 8.6 | 8.5 | 8.4 |
| KY 6b | 0.9 | -1.7 | -4.4 | 2.9 | 0.2 | 8.3 | 8.3 | 8.2 |
| KY 7a | 1.3 | -2.4 | -5.0 | 1.7 | 0.8 | 8.2 | 8.2 | 8.1 |
| KY 7b | 1.3 | -2.8 | -5.5 | 5.6 | 0.3 | 8.5 | 8.5 | 8.4 |
| KY 8 | 2.1 | -1.3 | n.a. | 6.2 | 1.0 | 8.6 | 8.5 | 8.4 |
| KY 9 | 3.2 | -2.6 | -5.0 | 7.3 | 0.0 | 8.6 | 8.6 | 8.5 |
| KY 10 | 3.5 | -1.0 | -4.2 | 8.1 | 0.3 | 8.7 | 8.6 | 8.6 |
| KY 10a | 8.6 | -1.4 | -7.8 | 13.8 | 0.8 | 9.1 | 9.0 | 8.9 |
| KY 11 | 19.3 | 0.0 | -4.3 | 14.2 | 0.2 | 9.1 | 9.0 | 9.0 |
| KY 13 | 29.5 | 1.3 | -7.3 | 7.8 | 0.7 | 8.7 | 8.6 | 8.5 |
| **Namibia** | **Congo Craton** | | | | | | | |
| **Khowarib Section** | | $\delta^{13}C$ | $\delta^{18}O$ | $\delta^{11}B$* | | A | B | C |
| Sample | meter | [‰] | [‰] | [‰] | | pH | pH | pH |
| KW1-10 | 0.0 | -3.2 | -7.4 | 9.7 | | 8.8 | 8.7 | 8.7 |
| KW1-11 | 0.1 | -3.2 | -7.3 | 6.7 | | 8.6 | 8.5 | 8.5 |
| KW1-12 | 0.2 | -3.2 | -6.1 | 3.2 | | 8.4 | 8.3 | 8.2 |
| KW1-14 | 0.6 | -3.0 | -7.2 | 2.8 | | 8.3 | 8.3 | 8.2 |
| KW1-15 | 0.8 | n.a. | n.a. | 3.5 | | 8.4 | 8.3 | 8.2 |
| KW1-18 | 1.4 | -3.1 | -7.7 | 1.7 | | 8.2 | 8.2 | 8.1 |
| KW1-18 | 1.4 | -3.1 | -7.7 | 1.5 | | 8.2 | 8.2 | 8.1 |
| KW1-21 | 2.7 | -2.9 | -7.6 | 2.0 | | 8.3 | 8.2 | 8.1 |
| KW1-24 | 4.3 | -3.0 | -7.7 | 1.5 | | 8.2 | 8.2 | 8.1 |
| KW1-29 | 6.8 | -2.8 | -7.5 | 2.7 | | 8.3 | 8.3 | 8.2 |

| | | | | | | | |
|---|---|---|---|---|---|---|---|
| KW1-32 | 8.3 | -3.0 | -7.5 | -0.1 | 8.1 | 8.0 | 7.9 |
| KW1-37 | 10.8 | -3.3 | -6.9 | -1.2 | 8.0 | 7.9 | 7.8 |
| KW1-45 | 14.8 | -4.2 | -9.0 | 0.5 | 8.2 | 8.1 | 8.0 |
| KW1-55 | 21.3 | -5.1 | -8.6 | 2.2 | 8.3 | 8.2 | 8.1 |
| KW1-58 | 31.3 | -5.2 | -9.1 | 0.2 | 8.1 | 8.0 | 7.9 |
| KW1-64 | 57.3 | -5.2 | -9.6 | 3.2 | 8.4 | 8.3 | 8.2 |
| KW1-67 | 80.3 | -5.2 | -9.5 | 2.5 | 8.3 | 8.2 | 8.2 |
| **Namibia** | **Congo Craton** | | | | | | |
| **Fransfontein Section** | | $\delta^{13}C$ | $\delta^{18}O$ | $\delta^{11}B$* | A | B | C |
| Sample | meter | [‰] | [‰] | [‰] | pH | pH | pH |
| FF1-2 | 0.2 | -1.6 | -7.0 | 3.0 | 8.3 | 8.3 | 8.2 |
| FF1-3 | 0.4 | -1.8 | -7.0 | 1.2 | 8.2 | 8.1 | 8.0 |
| FF1-4 | 0.6 | -2.2 | -7.3 | -0.5 | 8.1 | 8.0 | 7.9 |
| FF1-5 | 0.8 | -1.7 | -6.7 | -1.2 | 8.0 | 7.9 | 7.8 |
| FF1-6 | 1.0 | -2.6 | -7.3 | -2.6 | 7.8 | 7.7 | 7.5 |
| FF1-9 | 1.6 | -2.3 | -7.4 | 1.0 | 8.2 | 8.1 | 8.0 |
| FF1-12 | 2.2 | -3.0 | -7.5 | -2.2 | 7.9 | 7.8 | 7.6 |
| FF1-20 | 4.6 | -3.3 | -8.3 | -3.5 | 7.7 | 7.5 | 7.2 |
| FF1-22 | 5.4 | -2.8 | -8.8 | n.a. | | | |
| FF1-28 | 14.7 | -4.1 | -10.2 | -3.6 | 7.7 | 7.5 | 7.2 |
| FF1-29 | 42.0 | -4.4 | -9.7 | -2.0 | 7.9 | 7.8 | 7.6 |
| FF1-30 | 42.7 | -4.2 | -9.4 | -2.5 | 7.9 | 7.7 | 7.5 |
| FF1-31 | 48.2 | -0.3 | -6.9 | -4.3 | 7.6 | 7.3 | 6.6 |
| FF1-32 | 52.2 | 0.6 | -5.3 | -1.0 | 8.0 | 7.9 | 7.8 |
| FF1-34 | 72.2 | 1.5 | -1.5 | 2.0 | 8.3 | 8.2 | 8.1 |
| FF1-36 | 92.2 | 1.6 | -0.9 | 4.5 | 8.4 | 8.4 | 8.3 |
| FF1-37 | 102.2 | 1.6 | -5.0 | 6.7 | 8.6 | 8.5 | 8.5 |
| **Namibia** | **Congo Craton** | | | | | | |
| **Ombaatjie Section** | | $\delta^{13}C$ | $\delta^{18}O$ | $\delta^{11}B$* | A | B | C |
| Sample | meter | [‰] | [‰] | [‰] | pH | pH | pH |
| OBTJ 43 | 0.1 | 1.7 | -4.6 | 2.7 | 8.3 | 8.3 | 8.2 |
| OBTJ 45 | 1.5 | -2.6 | -6.3 | -3.3 | 7.7 | 7.6 | 7.3 |
| OBTJ 46 | 1.6 | -2.6 | -6.9 | -5.5 | 7.2 | 5.9 | - |
| OBTJ 47 | 2.5 | -3.0 | -6.9 | -4.8 | 7.4 | 7.1 | - |
| OBTJ 52 | 5.6 | -3.0 | -6.8 | -6.2 | 6.7 | - | - |
| OBTJ 55 | 10.5 | -3.9 | -8.5 | -6.0 | 6.9 | - | - |
| OBTJ 58 | 36.0 | -5.8 | -11.4 | -2.4 | 7.9 | 7.7 | 7.6 |
| OBTJ 65 | 106.0 | -4.1 | -8.9 | -0.2 | 8.1 | 8.0 | 7.9 |

**Table DR1:** Boron ($\delta^{11}B$ [‰, vs. NIST SRM 951]), carbonate carbon ($\delta^{13}C_{carb}$ [‰, vs. VPDB]) and oxygen ($\delta^{18}O$ [‰, vs. VPDB]) isotope data of all analyzed sections, including Namibia data (Kasemann et al., 2010). Uncertainty for Namibian B isotope data is $\delta^{11}B$*: ±1‰ $2\sigma_f$. A, B, C are pH estimations based on different $\delta^{11}B_{seawater}$ assumptions: $pK_B$ of 8.579 (Dickson, 1990), a fractionation factor $\alpha$ of 1.0272 (Klochko et al., 2006) and a seawater $\delta^{11}B$ composition of

A=20.5‰, B=21.5‰ and C=22.5‰ (same as Kasemann et al. (2010)) are used. The finally proposed $\delta^{11}B_{sw}$ composition of 20.5‰ is shaded in grey. n.a. = not analyzed.

---

**Table DR2:** Major and trace elements for the Chinese Xiaofenghe Section (NXF).

| Section | Height/ Sample | Al µg g$^{-1}$ | B µg g$^{-1}$ | Fe µg g$^{-1}$ | Mn µg g$^{-1}$ | S µg g$^{-1}$ | Si µg g$^{-1}$ | Sr µg g$^{-1}$ | Ca % | Mg % |
|---|---|---|---|---|---|---|---|---|---|---|
| NXF | 0.20 | 176 | 2 | 3763 | 2768 | 89 | 205 | 92 | 28 | 15 |
| NXF | 0.75 | 219 | 2 | 8813 | 2891 | 92 | 185 | 66 | 28 | 15 |
| NXF | 1.60 | 331 | 2 | 3348 | 1788 | 116 | 482 | 71 | 30 | 13 |
| NXF | 2.35 | 157 | 2 | 4574 | 2591 | 83 | 232 | 80 | 29 | 14 |
| NXF | 3.85 | 873 | 3 | 3320 | 2598 | 401 | 2243 | 87 | 32 | 12 |
| NXF | 4.80 | 158 | 3 | 11678 | 7065 | 90 | 193 | 64 | 28 | 15 |